# Enhancement of Hydrogen Gas Sensing of Nanocrystalline Nickel Oxide by Pulsed-Laser Irradiation

A. M. Soleimanpour,[†] Sanjay V. Khare,[‡] and Ahalapitiya H. Jayatissa*,[†]

[†]Nanotechnology and MEMS Laboratory, Department of Mechanical, Industrial and Manufacturing Engineering and [‡]Department of Physics and Astronomy, The University of Toledo, MS 312, Toledo, Ohio 43606-3390, United States

ABSTRACT: This paper reports the effect of post-laser irradiation on the gas-sensing behavior of nickel oxide (NiO) thin films. Nanocrystalline NiO semiconductor thin films were fabricated by a sol−gel method on a nonalkaline glass substrate. The NiO samples were irradiated with a pulsed 532-nm wavelength, using a Nd:YVO$_4$ laser beam. The effect of laser irradiation on the microstructure, electrical conductivity, and gas-sensing properties was investigated as a function of laser power levels. It was found that the crystallinity and surface morphology were modified by the pulsed-laser irradiation. Hydrogen gas sensors were fabricated using both as-deposited and laser-irradiated NiO films. It was observed that the performance of gas-sensing characteristics could be changed by the change of laser power levels. By optimizing the magnitude of the laser power, the gas-sensing property of NiO thin film was improved, compared to that of as-deposited NiO films. At the optimal laser irradiation conditions, a high response of NiO sensors to hydrogen molecule exposure of as little as 2.5% of the lower explosion threshold of hydrogen gas (40 000 ppm) was observed at 175 °C.

KEYWORDS: nickel oxide, laser irradiation, gas-sensing property, sol−gel coating
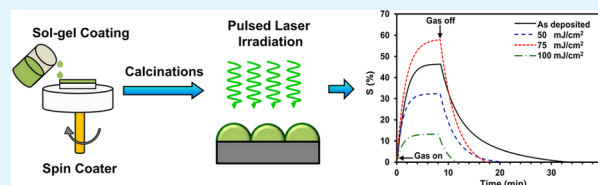
INTRODUCTION

The monitoring of hydrogen under ambient conditions is important, because of its wide range of applications in industries, laboratories, and energy storage. Industries are dealing with the transport, storage, and use of H$_2$ on a large scale. Therefore, there is a need for a stable, highly sensitive sensor for the monitoring and leak detection of H$_2$. Metal oxide gas sensors have been considered as an alternative replacement for current large and expensive analytical techniques, such as optical spectroscopy and gas chromatography.[1,2] Conventional metal oxide gas sensors consist of large polycrystalline grains where surface and grain boundaries are two causes of limiting their electrical transport phenomena.[3−5] The gas-sensing ability can be intensified by decreasing the grain size to nanoscale. In the past few years, nanostructured metal oxide gas sensors (NMOS), such as nickel oxide (NiO), zinc oxide (ZnO), and tin oxide (SnO$_2$), have attracted much attention, because of their high sensitivity and fast response and recovery.[6−10]

Nanostructured NiO semiconductors have been used in a variety of applications, such as transparent electrochromic film, super capacitors, fuel cell electrodes, and chemical gas sensors, because of their nontoxicity and high chemical stability.[10−13] NiO can be synthesized by various fabrication techniques, such as sol−gel, chemical vapor deposition (CVD), spray pyrolysis, and reactive sputter deposition.[14,15] Recent works related to H$_2$ detectors by Stamataki et al.[16] and Brilis et al.[17] reported the response of 15%−40% for 30 000 ppm H$_2$ at 200 °C for gas sensors that were fabricated by pulsed-laser deposition on silicon substrates. Steinebach et al. investigated NiO that was synthesized by radio frequency (RF) sputtering, and the response value of 55% was reported for 5000 ppm H$_2$ at 600

°C.[18] Laser modification of metal oxide thin films has been reported to improve different properties of the sample, such as electrical conductivity, carrier mobility, microstructure, and crystallinity.[5,13] Laser irradiation can be used to improve the surface of metal oxide thin film and increase sensor response.[19] Several appropriate uses of a laser have been introduced, such as application of a constant or pulsed-wave laser with different wavelengths to get the desired properties.

In this study, a post-fabrication modification by pulsed-laser irradiation of nanocrystalline is introduced to improve H$_2$ sensing of NiO thin films. The laser power is used to optimize the sensor response as a combination of higher response magnitude and faster response and recovery times. Nanostructured sol−gel samples were selected for this study for several reasons, such as small grain size (20 nm), high surface-to-volume ratio, and low operational temperature, compared to other conventional sensors. High response of these sensors, as well as faster response and recovery to H$_2$ exposure, can have a significant impact for industrial applications. Laser irradiation offers an additional tool to modify the microstructure of thin film such as crystallinity, grain size, and defects. This study is a continuation of our efforts to investigate and design a better metal oxide gas sensor by using laser modification of metal oxide surfaces. In an earlier study, this group showed that UV irradiation had an effect on the H$_2$ gas sensing of ZnO.[20]

■ EXPERIMENTAL SECTION

Nanocrystalline *p*-type NiO thin films were synthesized using a sol–gel technique. Nickel nitrate hexahydrate ($Ni(NO_3)_2 \cdot 6H_2O$) was dissolved in isopropanol alcohol and polyethylene glycol 200 to make 0.1 M solution by constant stirring at 25 °C. Nanoscale nickel hydroxide particles were produced in the solution by adding dilute ammonia into the stirring solution, in order to eliminate particle agglomeration; Triton X-100 was added to decrease surface tension in the solution. A very thin and uniform layer of solution was spread on a 2 cm × 2 cm nonalkaline glass substrate by spin coating at 1500 rpm for 20 s and 3000 rpm for 10 s. After coating each layer, the samples were heated to 350 °C for 5 min, to remove any organic compound in the film. Two layers were coated on the substrate to gain the proper thickness of the active layer. After coating two layers of sol–gel mixture, they were calcinated at 550 °C in a tube furnace for 3 h in air. The calcination process improved the microstructure and produced nanocrystalline NiO grains.

After the annealing step, the samples were subjected to laser irradiation by Nd:YVO$_4$ pulsed-laser system (pulsed width = 8 ns) with a wavelength of 532 nm, using an Osprey-532 laser source that was equipped with and controlled by an *X-Y* scanner. The laser beam with a window size of 20 μm × 20 μm was irradiated onto the film surface. The pulsing frequency of the laser system was fixed at 10 kHz, and the scanning speed was kept at 30 cm/s. The scanning pattern was designed and calibrated to yield three values for the laser irradiation: 50, 75, and 100 mJ/cm^2, respectively.

The X-ray diffraction (XRD) data were collected with a grazing-incidence X-ray diffraction (GID) technique with chromatized Cu Kα radiation, using 40 mA and 45 kV in the 2θ range of 35°–45° with a low incident angle of 0.9° (PANalytical, X-ray). The GID method preferentially probes the surface layer, and it causes an increase in the reflected intensity, compared to the regular XRD method. The XRD spectra were used to determine the crystallographic phases of the samples. Scanning electron microscopy (SEM) (Hitachi, Model S-4800) was used to study the surface morphology of NiO films before and after the post-laser-irradiation steps. The Fresnel approach was used to theoretically estimate the thickness of films.[17] A program was developed using Matlab software to theoretically estimate the refractive indices and the thickness of NiO film, based on the experimental values of the reflectance data from the bilayer of NiO/glass substrate. The value of the thickness for NiO films was estimated to be ~21 ± 3 nm.

The chemical binding energy analysis was performed on the surface of samples using XPS measurements (Kratos Axis Ultra XPS) with Al Kα radiation at 1486.6 eV and base vacuum of 2×10^{-10} mbar. To minimize the charging effect, a low-energy electron gun was used for charge neutralization. Corrections of energy shift, due to the steady-state charging, were made by assigning a binding energy of 284.6 eV to the C 1s peak.[21]

In order to fabricate sensor devices, the gold electrodes with a thickness of 50 nm were deposited by a vacuum thermal evaporation method, and subsequent photolithography was used to make electrodes with a comblike structure with a length of 200 μm and a space of 20 μm. The schematic diagram of the sensor and testing system is shown in Figure 1. The samples were mounted in a custom-built Pyrex chamber (200 cm^3) that has gas inlet and outlet to allow the gas to pass above the sample. The samples were placed on a resistive heater while the temperature was continuously controlled by a thermocouple. The carrier gas (dry air) was introduced to the chamber throughout the process. Various concentrations (1000–3000 ppm) of high-purity H$_2$ in dry air were introduced into the chamber using a mass flow meter. The time constant for gas exchange in the test chamber was ~15 s. The resistance between the electrodes was measured continuously using a Keithley Model 2001 multimeter in time intervals of 1 s, using Labview software.

■ RESULTS AND DISCUSSION

In general, fabricating nanosized grains in metal oxide is a vital step to gain a high-performance sensor with high response and
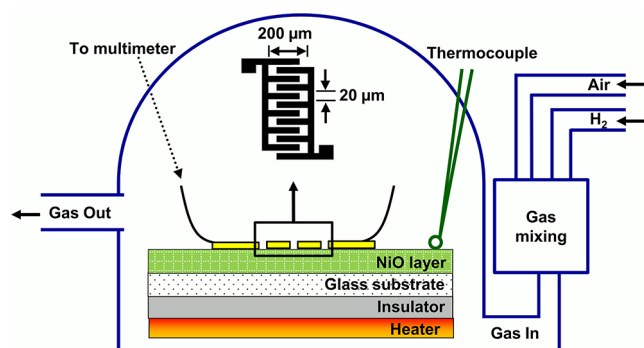

Figure 1. Schematic diagram of NiO sensor testing instrumentation. The inset is the top view of the sensor.

fast response and recovery.[22−24] In this study, nanocrystalline NiO is fabricated with using a sol–gel method.

By implementing an accurate concentration of a solution and optimum temperature, during the initial steps of preheating the sample, a random orientation of nuclei is initiated on the surface of the glass substrate. Furthermore, these nucleation sites can be converted to very fine NiO grains after the annealing step. During this stage, crystal planes that have lower energy and higher growth rates stabilize and form the final crystallographic structure of the grains.[25,26]

Figure 2 shows the XRD patterns of NiO films irradiated with different laser power levels. Both simple cubic phase and
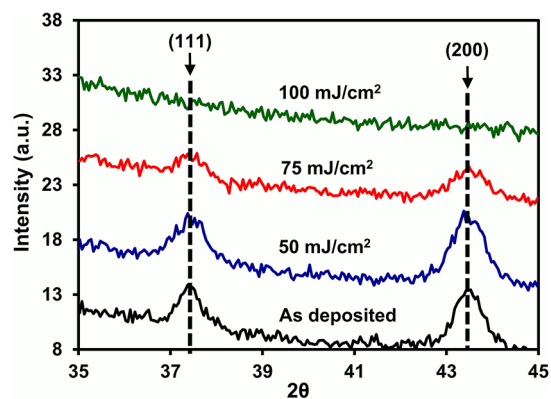
Figure 2. Grazing-incidence X-ray diffraction (GID) pattern of samples before and after laser irradiation.

face-centered cubic structure have been reported in the literature for sol–gel derived NiO films.[27,28] The diffraction patterns of our samples reveal two peaks, at 37.4° and 43.4°, which correspond to the (111) and (200) planes of simple cubic NiO, respectively. The (002) peak intensity is higher than that of the (111) peak. Moreover, the (111) and (200) peaks shifted toward a higher angle as the laser intensity increases (from 50 mJ/cm^2 to 75 mJ/cm^2), indicating that the films have a higher thermal stress induced by high laser power levels.[29] As the laser power increases to 75 and 100 mJ/cm^2, the crystallinity of the sample decreases. By calculating the full width at half-maximum (fwhm) for the (200) plane at 43.4°, the average grain size is calculated, using the Scherrer formula, to be ~20 nm.[30] However, because of some limiting factors in the GID method, the Scherrer formula cannot be used to evaluate an accurate crystal size of the sample;[31] therefore, additional investigations were carried out with SEM measure-
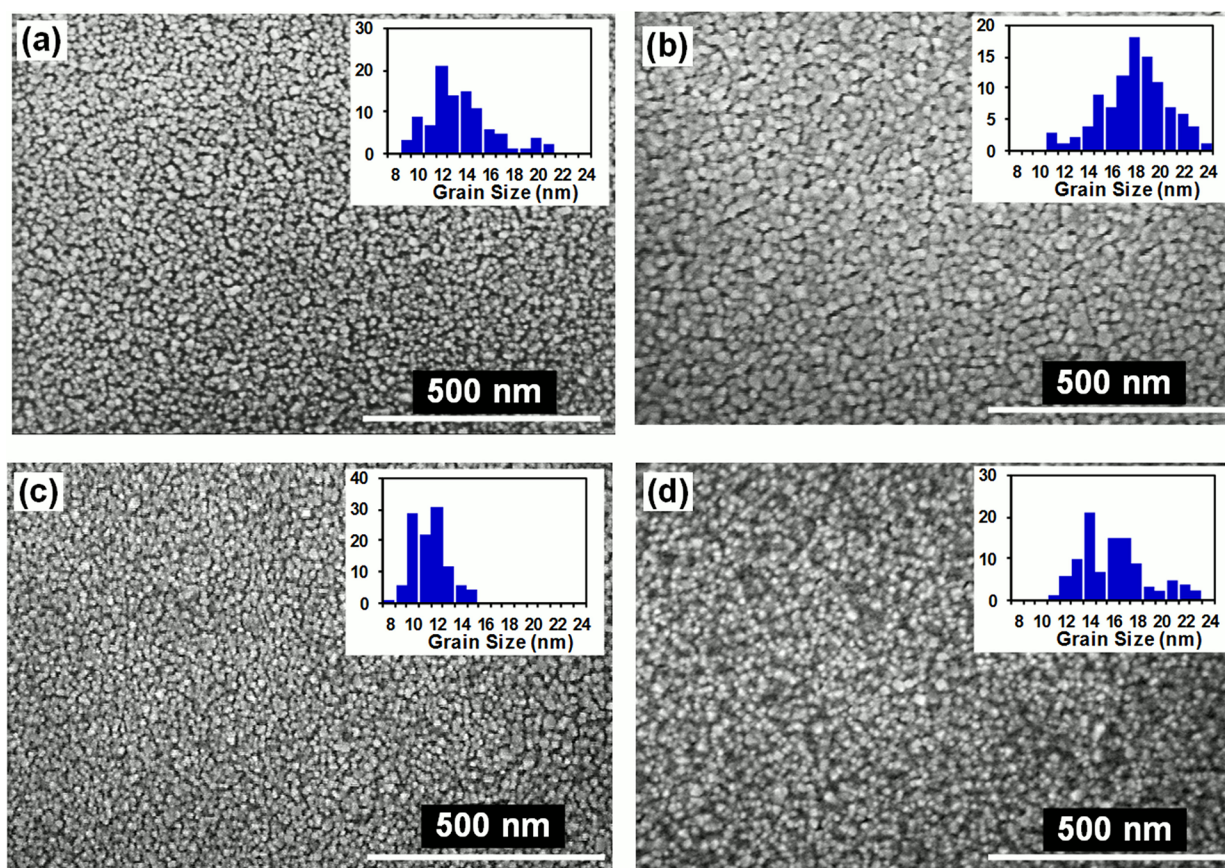
Figure 3. SEM images of nanocrystalline NiO on glass substrate with different laser powers: (a) as-deposited, (b) 50 mJ/cm^2, (c) 75 mJ/cm^2, and (d) 100 mJ/cm^2.

ments to investigate the surface morphology and the change of grain size in samples.

Figure 3 shows the SEM morphology of nanocrystalline NiO samples before and after laser irradiation. It can be clearly seen that the as-deposited film has spherical grains with a smooth coverage. As the laser power increases from 50 mJ/cm^2 to 100 mJ/cm^2, the surface morphology and the uniformity of thin film are changed. The average grain sizes of samples estimated using SEM data are 17.8, 29.9, 14.4, and 15.2 nm for the as-deposited and 50-, 75-, and 100-mJ/cm^2 irradiated samples, respectively. The surface-to-volume ratio and degree of crystallinity are two parameters that play an important role in the gas sensing of NiO thin films.[32,33] The grain size increases slightly by using 50 mJ/cm^2, which can enhance the electrical conductivity throughout the grains.[34] The corresponding XRD pattern in Figure 3b also represents higher peak intensities for this sample. By applying a higher laser power of 75 mJ/cm^2, the grain size decreases, as shown in Figure 3c. Moreover, as the laser power is increased to 100 mJ/cm^2, the grain size is slightly changed and the degree of crystallinity is degraded significantly, as shown in Figure 3d. The grain size histogram was inserted in Figure 3 to better exhibit the grain size distribution in each sample.

The results from Figures 2 and 3 show that the power level of laser beam can be used to optimize the size of grains and maximize the film uniformity of as-deposited NiO thin films. As the laser intensity (I) increases from zero toward a critical threshold (I_c), the laser functions as a heat source to heal defects in the grains and, thus, cause an increase in the size and uniformity of grains. When $I > I_c$, the laser heat is adequate to start local melting of several NiO layers.[35] For laser intensities greater than I_c, crystallinity is completely degraded and an amorphous phase is created. As a result, an optimization of laser power is required to get the best combination of grain size, porosity level, and crystallinity of NiO thin film for gas-sensing applications.

The XPS measurement reveals the chemical states of bonded atoms.[36] Figures 4a and 4b show the XPS spectra of as-deposited and 75 mJ/cm^2 laser-irradiated samples, respectively, for the Ni 2p and O 1s ranges. The peaks for the as-deposited sample obtained at binding energies of 854.8 eV (Ni 2p$_{3/2}$) and 873.9 eV (Ni 2p$_{1/2}$) suggest the presence of NiO.[37] For 75 mJ/cm^2-laser-irradiated sample, the Ni 2p$_{3/2}$ peak at 854.7 eV and the Ni 2p$_{1/2}$ peak at 874.2 eV indicate the presence of NiO. Satellite peaks appear at the 861−862 eV (Ni 2p$_{3/2}$) and 879−881 eV (Ni 2p$_{1/2}$) because of the shakeup processes.[37] It is clear that the portion of Ni 2p$_{3/2}$ at 856.7 eV that corresponds to Ni^{3+} increases with laser irradiation. Figure 4b shows the O 1s spectrum and two peaks that are clearly separated, which correspond to the binding states of Ni^{2+} (530.2 eV) and Ni^{3+} (532.3 eV).[38] It is known that nonstoichiometric NiO contains Ni^{2+} vacancies and, to keep the charge neutral, some Ni^{2+} should be oxidized to Ni^{3+}; hence, the presence of Ni$_2$O$_3$ confirms the nonstoichiometric of NiO samples.[21,39] It can be seen clearly that the portion of O 1s from Ni^{2+} decreases with laser irradiation and gives rise to an O 1s peak at 532.3 eV, which corresponds to Ni$_2$O$_3$. The concentration of the peak decreased and the intensities of both peaks are on the same level. These results suggest that NiO partially turns to Ni$_2$O$_3$ when the films were laser-irradiated.
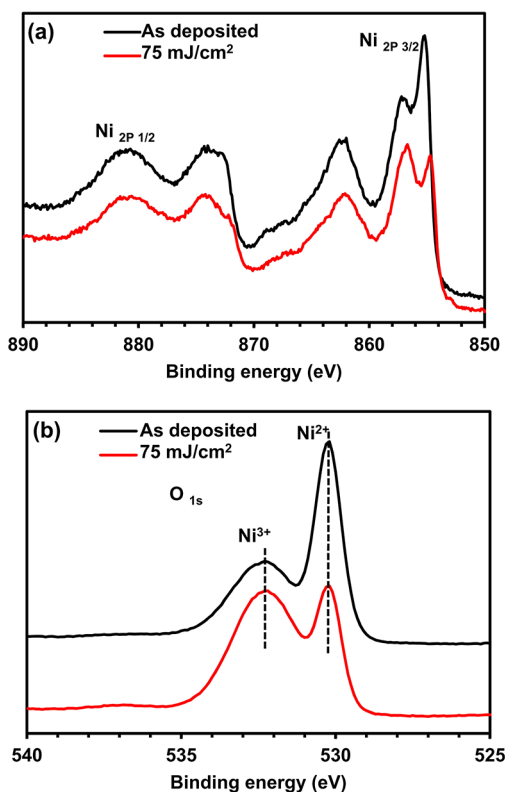
Figure 4. XPS spectra of at the original surfaces of as-deposited and 75 mJ/cm² laser-irradiated samples in the (a) Ni 2p and (b) O 1s ranges.

The electrical properties of NiO thin films were characterized by collecting the change in resistance with temperature in the range of 25−250 °C. The conductivity (σ) varies with temperature in a classical Arrhenius form:[40]

$$\sigma = \sigma_0 \exp\left(\frac{E_a}{kT}\right) \tag{1}$$

Here, σ_0 is the conductivity at high temperature, E_a the activation energy, and k the Boltzmann constant. Figure 5 shows a semilogarithmic plot of σ versus the inverse of the absolute temperature ($1/T$). This monotonic increase in σ with increasing T is a well-known semiconductor behavior.[41,42] It can be seen that the conductivity of NiO films increases by laser irradiation at 50 mJ/cm² and significantly decreases by
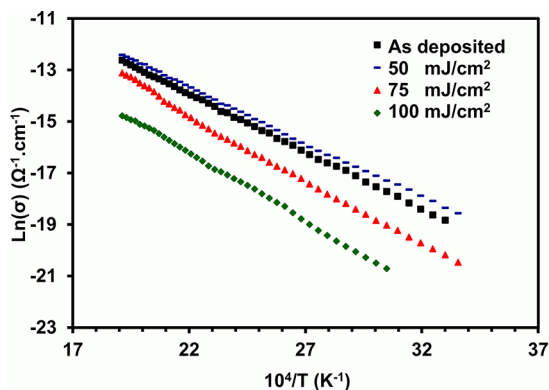
Figure 5. Semilogarithmic plot of the conductivity (σ) versus reciprocal of the absolute temperature ($1/T$) of NiO films before and after laser irradiation.

increasing the laser power to 75 and 100 mJ/cm². As an example, the values of σ, in units of $10^5 \, \Omega^{-1} \, cm^{-1}$ at 100 °C, are 1.00, 1.34, 0.3, and 0.07 for the as-deposited, 50-, 75-, and 100-mJ/cm² laser-irradiated samples, respectively. A decrease in conductivity with increased laser annealing was reported for a SnO₂ gas sensor.[43] Activation energies can be obtained from fitting the Arrhenius equation to the data in Figure 5. The calculated E_a values are 0.38, 0.37, 0.43, and 0.45 eV for the as-deposited, 50-, 75-, and 100-mJ/cm² laser-irradiated samples, respectively. It is noticed that, for the sample with laser irradiation at 50 mJ/cm², the activation energy is the lowest. This is consistent with the structural data shown in Figures 2 and 3, where the crystallinity increases for the 50 mJ/cm²-irradiated sample and the crystallinity decreases upon increasing the laser power further to 100 mJ/cm². The activation energy has been attributed to the tunneling of charge carriers among NiO grains.[44] The sample with the highest crystallinity has the lowest value for E_a.

The H₂ gas response of NiO thin films irradiated by different laser power levels were investigated by measuring the resistance versus time over two electrodes for a constant temperature. The samples were tested at different temperatures between 150 °C and 225 °C. It was found that the best response of NiO for H₂ was exhibited at 175 °C. All data that are discussed further were collected at this temperature. The sensor response was calculated based on

$$S \, (\%) = \frac{R_{gas} - R_{ref}}{R_{ref}} \times 100 \tag{2}$$

where R_{gas} and R_{ref} are the resistances of sensor with and without the target gas (H₂), respectively. After H₂ gas was introduced into the chamber, the sensor resistance increased and reached to a saturation level and, by purging H₂ gas from the chamber, the resistance returned to its original value. The same behavior intensified by exposing the samples to higher H₂ concentrations.

The H₂ sensing mechanism of NiO can be attributed to the nonstoichiometry of percentage of Ni²⁺ and O²⁻ in the prepared samples. Vacancies that are located in cation sites can form holes. Oxygen molecules can absorb on the surface of grains and produce oxygen ions.[44,45] When oxygen ions adsorb on the surface of NiO grains, they act as an acceptor and force electrons to be removed from the grains and produce extra holes in the lattice. As a result of this reaction, the resistance of the samples decreases by increasing the hole concentration.[46,47] By exposing the samples to a reducing gas such as H₂, the H₂ molecules react with adsorbed oxygen and release electrons back to the lattice. Therefore, hole concentration in the lattice decreases and the resistance of the film increases, which is normal p-type semiconductor behavior.[48] The reaction summaries are as follows:[48−50]

$$O_{2(Adsorbed)} + 2\bar{e} \leftrightarrow 2O^- \tag{3}$$

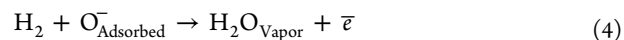$$H_2 + O^-_{Adsorbed} \rightarrow H_2O_{Vapor} + \bar{e} \tag{4}$$

Figure 6a shows the sensor response to H₂ concentrations of 1000, 2000, and 3000 ppm in the air for all samples. It can be seen that, by increasing the H₂ concentration, the response values increases for all samples. In the sample that was irradiated with low laser power (50 mJ/cm²), the response decreases due to its larger grain size and decrease in surface-to-volume ratio. By further increasing the laser power to 75 mJ/
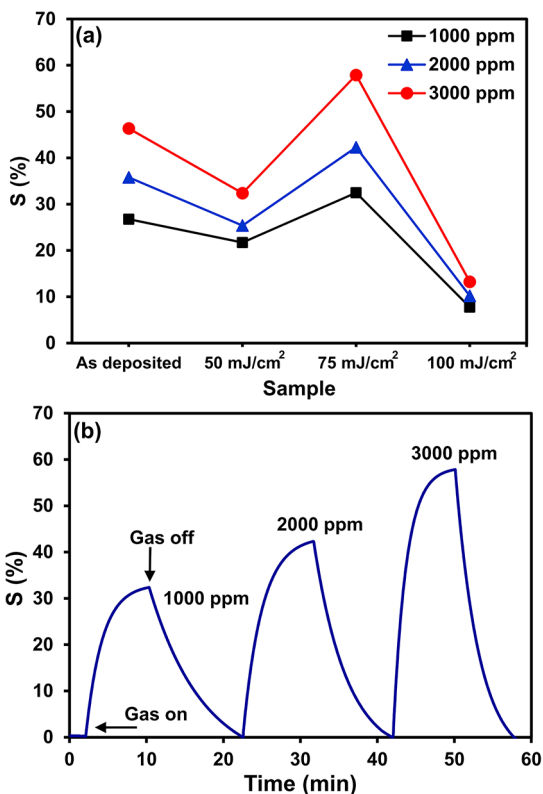
Figure 6. (a) Response of NiO samples at 175 °C for different H_2 concentration of 1000, 2000, and 3000 ppm. (b) Response values for 1000, 2000, and 3000 ppm H_2 gas at 175 °C for the 75-mJ/cm² laser-irradiated sample.

cm^2, the sample possesses the highest response, compared to all samples. This phenomenon can be attributed to smaller grain size and higher uniformity of NiO film irradiated at 75 mJ/cm². Figure 6b shows the experimental response values for 1000, 2000, and 3000 ppm of H_2 gas at 175 °C for the 75-mJ/cm² laser-irradiated sample. Furthermore, as the laser power is increased to 100 mJ/cm², the response decreases as a result of a degradation of crystallinity.

The experimentally measured responses (S) of the sensors were fitted with a theoretical model as the first-order time-step response with exponential rise and fall functions. The equations for the sensor response S are given by[51]

$$\frac{R}{R_0} = \exp\left(\frac{t}{\tau_1}\right) \qquad 0 \leq t \leq t_1 \tag{5}$$

$$\frac{R}{R_0} = \exp\left(\frac{t_1}{\tau_1}\right) \times \exp\left(\frac{t - t_2}{\tau_2}\right) \qquad t_1 \leq t \leq t_2 \tag{6}$$

Here, R_0 is the initial resistance of the sensor, t_1 is the time when the gas is turned off, t_2 is the time when the sensor recovers to its original value, and τ_1 and τ_2 are transient times for response and recovery processes, respectively. Transient time was defined as the time needed for the sensor to reach 63% of its initial value. Separate fits to the curve before and after t_1 were done to determine τ_1 and τ_2. Figure 7 shows the experimental values for response and first-order exponential fit for 1000 ppm H_2 gas at 175 °C of a NiO sample irradiated with 75 mJ/cm² laser power. By comparison of the experimental data and first-order response, it can be seen that the fitted
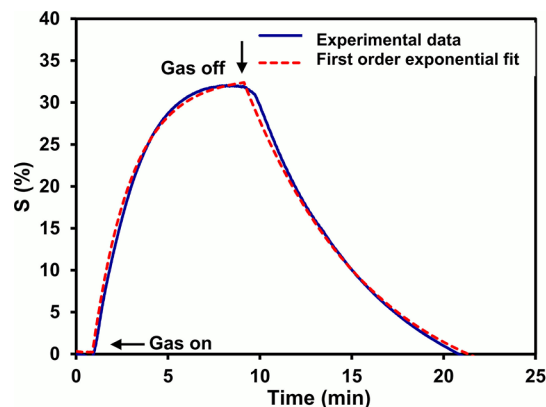
Figure 7. Real response and first-order exponential fit for 1000 ppm H_2 gas at 175 °C of the 75-mJ/cm² laser-irradiated NiO sample.

values are within 95% accuracy of experimental values. Figures 8a and 8b show the fitted data for H_2 gas response of NiO
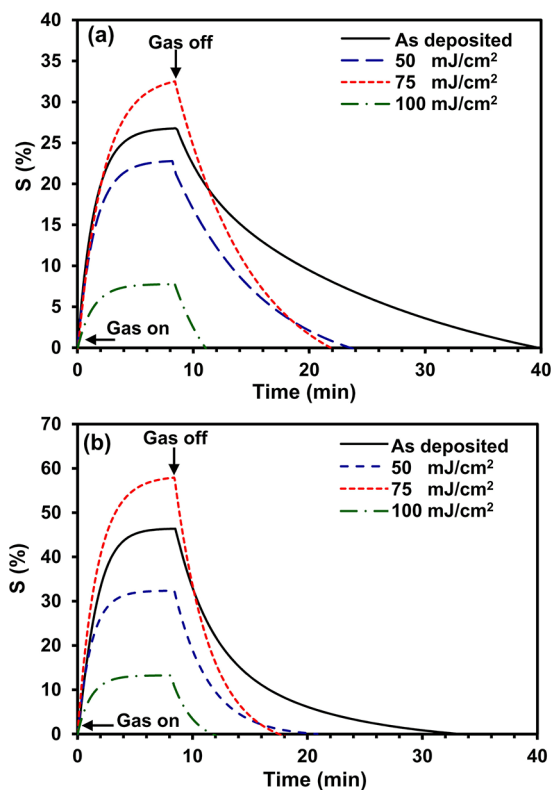
Figure 8. Response of all samples at 175 °C for different H_2 concentrations: (a) 1000 ppm and (b) 3000 ppm.

samples for two different H_2 concentrations of 1000 and 3000 ppm at 175 °C. Table 1 shows the values of S, τ_1, and τ_2 for all samples exposed to different H_2 concentrations at 175 °C. These concentrations, which have a safety factor of 10 (low explosion limit of H_2, 40 000 ppm), were selected for the H_2 concentrations in this experiment. The highest response for 1000−3000 ppm H_2 gas was measured for the 75 mJ/cm² sample. Moreover, this sample has a response time of τ_1= 134 s, which is also the highest of the set for 1000 ppm of H_2 at 175 °C. On the other hand, the recovery times decrease monotonically while going from the as-deposited sample to laser-irradiated samples, and decrease further by increasing the

**Table 1. S, τ_1, and τ_2 Values for Different Samples**

sample	H_2 (10^3 ppm)	Response, S (%)	Response time, τ_1 (s)	Recovery time, τ_2 (s)
as-deposited	1	26.7	87	788
	2	35.8	85	446
	3	46.3	81	322
50 mJ/cm^2	1	21.7	87	471
	2	25.4	80	225
	3	32.3	71	181
75 mJ/cm^2	1	32.4	134	406
	2	42.3	128	259
	3	57.9	101	187
100 mJ/cm^2	1	7.7	80	229
	2	10.2	79	145
	3	13.2	67	117

Figure 9. (a) Repeatability of the 75-mJ/cm^2 laser-irradiated sample for 1000 ppm of H_2 gas at 175 °C. (b) Response values of different test numbers for the as-deposited and 75-mJ/cm^2 laser-irradiated NiO sample for 1000 ppm H_2 gas at 175 °C.

laser power. The τ_1 and τ_2 values decreases by increasing H_2 concentration for all samples, which can be described by increasing H_2 molecules and limited available sites on the surface of grains.

The sensor characteristics of the 75 mJ/cm^2 laser-irradiated sample were improved, compared with the as-deposited sample: the response values improved by ~21% for 1000 ppm of H_2 and 24% for 3000 ppm of H_2. The effect of using optimized laser power to improve sensor response is not a special case for these NiO samples. The same study was done for thicker NiO films doped with lithium and ZnO thin films derived from the sol−gel method. In both cases, this group found similar trends to optimize sensor response for H_2 detection with laser irradiation. Detailed results for these experiments will be reported elsewhere. These data demonstrate the generality of our results for other types of semiconducting oxide films.

The sensing properties of samples are determined by two competing parameters of high conductivity, which correlates with high crystallinity and also high surface-to-volume ratio for higher adsorption of H_2 gas molecules. It can be seen that low laser power decreases the response, as a result of an increase in grain size and crystallinity and, therefore, a decrease in surface-to-volume ratio. As a result, the exposed area decreases, which is consistent with the SEM observation from Figure 3. However, the rise in crystallinity causes an increase in conductivity, as seen in Figure 5. By further increasing the laser power to 75 mJ/cm^2, the response increases, compared to the as-deposited sample, because of its higher uniformity and smaller grain sizes, as evidenced from the SEM images from Figure 3c and lower conductivity (Figure 5). By using a laser power of 100 mJ/cm^2, the grain crystallinity degrades significantly and the samples show low sensitivity to H_2 gas. It is well-known that samples with more porosity have higher sensitivity. Thus, there is a competition between increasing crystallinity but decreasing the porosity with high laser power. Therefore, there is an intermediate power level (in this case, 75 mJ/cm^2), which can improve the gas-sensing property of NiO samples and decrease the recovery time.

Repeatability is a critical factor for commercial gas sensors, which need to work for long periods of time without the need for replacement and recalibration.[18,52] Figure 9a shows the repeatability data for the laser-irradiated sample for 1000 ppm
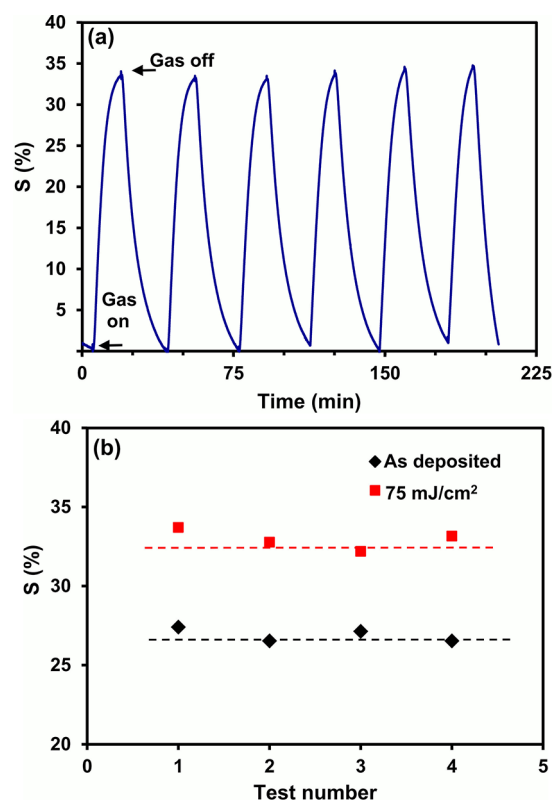
H_2 gas at 175 °C. A highly repeatable behavior is observed for the sample. Small deviation can be attributed to the small changes in the concentration of target gas using mass flow meters. The samples also were tested at different times to address reliability issues. It was found that the samples show the similar sensing behavior over time. Figure 9b shows the response values for different measurements. It is shown that the response values are almost comparable over time.

■ CONCLUSION

In summary, a nanocrystalline NiO sensor can be used for H_2 gas detection at lower temperature than conventional metal oxide gas sensors. This lowering of the sensing temperature can be beneficial in many industrial applications. This oxide has several advantages of high response, and fast response and recovery. In this study, pulsed-laser irradiation on NiO film was employed to improve its gas-sensing properties. Different laser power levels have been tested to understand the effect of laser irradiation on the gas-sensing behavior of NiO sample. At optimal laser power levels, the laser-irradiated samples have higher response and faster recovery than the as-deposited sample. The results of this investigation suggest that the laser irradiation technique is a general and applicable method for NiO-based gas sensors. Furthermore, authors believe that this study will influence further improvement of metal oxide gas sensors by laser treatments in the future.

■ AUTHOR INFORMATION

Corresponding Author
*E-mail: ajayati@utnet.utoledo.edu.

4656

dx.doi.org/10.1021/am301024a | ACS Appl. Mater. Interfaces 2012, 4, 4651−4657

■ REFERENCES

(1) Choi, J. K.; Hwang, I. S.; Kim, S. J.; Park, J. S.; Park, S. S.; Jeong, U.; Kang, Y. C.; Lee, J. H. *Sens. Actuators, B* **2010**, *150*, 191−199.

(2) Wetchakun, K.; Samerjai, T.; Tamaekong, N.; Liewhiran, C.; Siriwong, C.; Kruefu, V.; Wisitsoraat, A.; Tuantranont, A.; Phanichphant, S. *Sens. Actuators, B* **2011**, *160*, 580−591.

(3) Kumagai, H.; Matsumoto, M.; Toyoda, K.; Obara, M. *J. Mater. Sci. Lett.* **1996**, *15*, 1081−1083.

(4) Kitao, M.; Izawa, K.; Urabe, K.; Komatsu, T.; Kuwano, S.; Yamada, S. *Jpn. J. Appl. Phys.* **1994**, *33*, 6656−6662.

(5) Yoshimura, K.; Miki, T.; Tanemura, S. *Jpn. J. Appl. Phys.* **1995**, *34*, 2440−2446.

(6) Nagase, T.; Ooie, T.; Sakakibara, J. *Thin Solid Films* **1999**, *357*, 151−158.

(7) Bhaumik, G. K.; Nath, A. K.; Basu, S. *Materials Science and Engineering: B* **1998**, *52*, 25−31.

(8) Fasaki, I.; Giannoudakos, A.; Stamataki, M.; Kompitsas, M.; György, E.; Mihailescu, I. N.; Roubani-Kalantzopoulou, F.; Lagoyannis, A.; Harissopulos, S. *Appl. Phys. A: Mater. Sci. Process.* **2008**, *91*, 487−492.

(9) Mishra, V. N.; Agarwal, R. P. *Sens. Actuators, B* **1994**, *21*, 209−212.

(10) Jennifer, S. O.; Hung-Ta, W.; Byoung, S. K.; Zhuangchun, W.; Fan, R.; Andrew, G. R.; Stephen, J. P. *Nanotechnology* **2005**, *16*, 2218.

(11) Singh, J.; Kalita, P.; Singh, M. K.; Malhotra, B. D. *Appl. Phys. Lett.* **2011**, *98*, 123702−3.

(12) Hoey, M. L.; Carlson, J. B.; Osgood, R. M.; Iii; Kimball, B.; Buchwald, W. *Appl. Phys. Lett.* **2010**, *97*, 153104−3.

(13) Hotovy, I.; Huran, J.; Spiess, L.; Capkovic, R.; Hascik, S. *vacuum* **2000**, 300−307.

(14) Matsumiya, M.; Qiu, F.; Shin, W.; Izu, N.; Murayama, N.; Kanzaki, S. *Thin Solid Films* **2002**, *419*, 213−217.

(15) Patil, P. S.; Kadam, L. D. *Appl. Surf. Sci.* **2002**, *199*, 211−221.

(16) Stamataki, M.; Tsamakis, D.; Brilis, N.; Fasaki, I.; Giannoudakos, A.; Kompitsas, M. *Phys. Status Solidi A* **2008**, *205*, 2064−2068.

(17) Brilis, N.; Foukaraki, C.; Bourithis, E.; Tsamakis, D.; Giannoudakos, A.; Kompitsas, M.; Xenidou, T.; Boudouvis, A. *Thin Solid Films* **2007**, *515*, 8484−8489.

(18) Steinebach, H.; Kannan, S.; Rieth, L.; Solzbacher, F. *Sens. Actuators, B* **2010**, *151*, 162−168.

(19) Zhang, C.; Van Overschelde, O.; Boudiba, A.; Snyders, R.; Olivier, M.-G.; Debliquy, M. *Mater. Chem. Phys.* **2012**, *133*, 588−591.

(20) Soleimanpour, A. M.; Hou, Y.; Jayatissa, A. H. *Appl. Surf. Sci.* **2011**, *257*, 5398−5402.

(21) Sasi, B.; Gopchandran, K. G. *Nanotechnology* **2007**, *18*, 115613.

(22) Yoo, K. S.; Park, S. H.; Kang, J. H. *Sens. Actuators, B* **2005**, *108*, 159−164.

(23) Comini, E. *Anal. Chim. Acta* **2006**, *568*, 28−40.

(24) Aslani, A.; Oroojpour, V.; Fallahi, M. *Appl. Surf. Sci.* **2011**, *257*, 4056−4061.

(25) Chang, J. F.; Kuo, H. H.; Leu, I. C.; Hon, M. H. *Sens. Actuators, B* **2002**, *84*, 258−264.

(26) Liu, X. *J. Appl. Phys.* **2004**, *95*, 3141.

(27) Hotovy, I.; Rehacek, V.; Siciliano, P.; Capone, S.; L., S. *Thin Solid Films* **2002**, *4810*, 9−15.

(28) Chandrappa, K. G.; Venkatesha, T. V.; Nayana, K. O.; Punithkumar, M. K. *Mater. Corros.* **2011**, *63*, 445−455.

(29) Mallikarjuna Reddy, A.; Sivasankar Reddy, A.; Sreedhara Reddy, P. *Vacuum* **2011**, *85*, 949−954.

(30) Patterson, A. L. *Phys. Rev.* **1939**, *56*, 978−982.

(31) Smilgies, D. M. *J. Appl. Crystallogr.* **2009**, *42*, 1030−1034.

(32) Wang, C.; Yin, L.; Zhang, L.; Xiang, D.; Gao, R. *Sensors* **2010**, *10*, 2088−106.

(33) Devi, G. S.; Hyodo, T.; Shimizu, Y.; Egashira, M. *Sens. Actuators, B* **2002**, *87*, 122−129.

(34) Korotcenkov, G. *Mater. Sci. Eng., R* **2008**, *61*, 1−39.

(35) Tsang, W. M.; Wong, F. L.; Fung, M. K.; Chang, J. C.; Lee, C. S.; Lee, S. T. *Thin Solid Films* **2008**, *517*, 891−895.

(36) Grosvenor, A. P.; Biesinger, M. C.; Smart, R. S. C.; McIntyre, N. S. *Surf. Sci.* **2006**, *600*, 1771−1779.

(37) Kim, K. S.; Winograd, N. *Surf. Sci.* **1974**, *43*, 625−643.

(38) Oswald, S.; Brückner, W. *Surf. Interface Anal.* **2004**, *36*, 17−22.

(39) Nandy, S.; Saha, B.; Mitra, M.; Chattopadhyay, K. *J. Mater. Sci.* **2007**, *42*, 5766−5772.

(40) Aydogdu, G. H.; Ruzmetov, D.; Ramanathan, S. *J. Appl. Phys.* **2010**, *108*, 113702−6.

(41) Martin, S. W.; Martin, D. M.; Schrooten, J.; Meyer, B. M. *J. Phys.: Condens. Matter* **2003**, *15*, S1643.

(42) Jayatissa, A. H.; Samarasekara, P.; Kun, G. *physica status solidi (a)* **2009**, *206*, 332−337.

(43) Steiner, K.; Sulz, G.; Neske, E.; Wagner, E. *Sens. Actuators, B* **1995**, *26*, 64−67.

(44) Chang, S. J.; Weng, W. Y.; Hsu, C. L.; Hsueh, T. J. *Nano Communication Networks* **2010**, *1*, 283−288.

(45) Dirksen, J. A.; Duval, K.; Ring, T. A. *Sens. Actuators, B* **2001**, *80*, 106−115.

(46) S. M.SZE, *semiconductor devices*. john wiley&sons: 1985; p 523.

(47) Cappus, D.; HaBel, M.; Neuhaus, E.; Heber, M.; Rohr, F.; Freund, H. J. *Surf. Sci.* **1995**, *337*, 268−277.

(48) Liu, B.; Yang, H.; Zhao, H.; An, L.; Zhang, L.; Shi, R.; Wang, L.; Bao, L.; Chen, Y. *Sens. Actuators, B* **2011**, *156*, 251−262.

(49) Wu, J. B.; Nan, J.; Nan, C. W.; Lin, Y.; Deng, Y.; Zhao, S. *Materials Science and Engineering: B* **2003**, *99*, 294−297.

(50) Moseley, P. T., *Thick film semiconductor gas sensors*. Elsevier: Amsterdam, 1994.

(51) Gautam, M.; Jayatissa, A. H. *Mater. Sci. Eng., C* **2011**, *31*, 1405−1411.

(52) Meixner, H.; Lampe, U. *Sens. Actuators, B* **1996**, *33*, 198−202.

4657

dx.doi.org/10.1021/am301024a | *ACS Appl. Mater. Interfaces* 2012, 4, 4651−4657